Journal of Solid State Chemistry 183 (2010) 2746–2758

Contents lists available at ScienceDirect

Journal of Solid State Chemistry

journal homepage: www.elsevier.com/locate/jssc

Investigation of the stability of Co-doped apatite ionic conductors in NH_3

D.A. Headspith [a], A. Orera [b], P.R. Slater [c], N.A. Young [a], M.G. Francesconi [a,*]

[a] Department of Chemistry, University of Hull, Cottingham Road, Hull HU6 7RX, UK
[b] Instituto de Ciencia de Materiales de Aragón, Dpto de Ciencia y Tecnología de Materiales y Fluidos Ed. Torres, Quevedo c/María de Luna 3, 50018 Zaragoza, Spain
[c] School of Chemistry, University of Birmingham, Birmingham B15 2TT, UK

ARTICLE INFO

Article history:
Received 27 May 2010
Received in revised form
26 August 2010
Accepted 27 August 2010
Available online 8 October 2010

Keywords:
Apatite
Ammonia
Solid oxide fuel cell

ABSTRACT

Hydrogen powered solid oxide fuel cells (SOFCs) are of enormous interest as devices for the efficient and clean production of electrical energy. However, a number of problems linked to hydrogen production, storage and transportation are slowing down the larger scale use of SOFCs. Identifying alternative fuel sources to act as intermediate during the transition to the full use of hydrogen is, therefore, of importance. One excellent alternative is ammonia, which is produced on a large scale, is relatively cheap and has the infrastructure for storage and transportation already in place. However, considering that SOFCs operate at temperatures higher than 500 °C, a potential problem is the interaction of gaseous ammonia with the materials in the cathode, anode and solid electrolyte. In this paper, we extend earlier work on high temperature reactions of apatite electrolytes with NH_3 to the transition metal (Co) doped systems, $La_{9.67}Si_5CoO_{26}$ and $La_{10}(Si/Ge)_5CoO_{26.5}$. A combination of PXRD, TGA and XAFS spectroscopy data showed a better structural stability for the silicate systems. Apatite silicates and germanates not containing transition metals tend to substitute nitride anions for their interstitial oxide anions, when reacted with NH_3 at high temperature and, consequentially, lower the interstitial oxide content. In $La_{9.67}Si_5CoO_{26}$ and $La_{10}(Si/Ge)_5CoO_{26.5}$ reduction of Co occurs as a competing process, favouring lower levels of nitride–oxide substitution.

1. Introduction

Apatite-type materials have recently been investigated for their oxide ion conductivity and, hence, applicability as an electrolyte in areas such as solid oxide fuel cells (SOFCs) [1]. Hydrogen powered SOFCs are of enormous interest as devices for the production of clean energy. However, a number of problems linked to hydrogen production, storage and transportation are slowing down the large scale use of SOFCs.

Hydrogen is a potentially explosive gas, making handling and transport difficult for large scale technological applications. Therefore, there is growing interest in alternative fuels, one example being ammonia, as a carbon free fuel source with a similar performance to hydrogen [2]. The use of ammonia in fuel cells can potentially yield only N_2 and H_2O emissions and hence reduce greenhouse gas emissions, relative to burning fossil fuels [3]. Ammonia is currently produced in large quantities, with well established storage and distribution infrastructure because of its importance in the fertiliser industry. It can be liquefied under relatively mild conditions (10 atmospheres of pressure, or at −33 °C at atmospheric pressure) for transport or alternatively dissolved in water for safe delivery [2–4].

While ammonia cannot be used in low temperature polymer fuel cells, due to poisoning of the system, this is not a problem with high temperature cells, and in this respect ammonia has been demonstrated by a number of groups as a suitable fuel for use in solid oxide fuel cells [5]. There is still, however, a need for fundamental studies of the interaction of NH_3 fuels with materials in the cell. In particular, high temperature heat treatment in NH_3 is a known route for the synthesis of oxide nitrides, [6,7] and consequently it is possible that use of NH_3 may lead to nitridation occuring on the anode side of the cell under operating conditions. In this respect, it has been recently shown that NH_3 heat treatment will lead to significant nitridation of CeO_2 and the apatite-type oxide ion conductors $(La/Sr)_{10-x}Si_6O_{26+z}$ [8–10]. The latter apatite systems are new electrolytes for potential use in solid oxide fuel cells [11–15]. They are non-conventional electrolytes in the sense that the oxide ion conduction proceeds via interstitial oxide ions, in contrast to the traditional fluorite and perovskite systems, which are vacancy mediated oxide ion conductors.

Apatite materials take the general formula $A_{10}(MO_4)_6X_2$, where A is an alkali, alkaline earth, rare-earth metal, lead or bismuth, M is silicon, germanium, phosphorus or vanadium and X is oxygen, fluorine, chlorine, bromine, iodine or hydroxide. The apatite structure (Fig. 1) consists of isolated MO_4 units with A cations in

* Corresponding author.
E-mail address: m.g.francesconi@hull.ac.uk (M.G. Francesconi).

0022-4596/$ - see front matter © 2010 Elsevier Inc. All rights reserved.
doi:10.1016/j.jssc.2010.08.033

both nine and seven coordinate sites. The *X* anions also run in linear chains along the *c*-axis located at the cell edge. In terms of the application of apatites as oxide ion conductors, in particular those where *A*=rare earth (typically La), *M*=Si or Ge, *X*=O, it is the presence of interstitial oxide ions which is of vital importance. These interstitial oxide anions are located at the oxide channel periphery, close to the MO_4 tetrahedra, either as Frenkel-type defects or as oxygen hyperstoichiometry [16].

In our previous work, we showed that heat treatment of the apatite systems, $La_{9.33}Si_6O_{26}$ and, $La_{8+x}Sr_{2-x}(Si/Ge)_6O_{26+x/2}$, in NH_3 led to nitridation of both oxides, with the level of nitridation increasing with increasing temperature (600–950 °C) [9,10]. These results also suggested that the apatites can accommodate nitride anions into the oxide anion channel, which runs along the *c*-axis of these materials, with the displacement of oxygen. These channels are also a suitable place for the resulting oxide anion vacancies arising from ammonolysis of apatites which are initially oxygen stoichiometric, i.e. those containing 26 oxide anions per formula unit. Investigation into the strontium-doped samples, containing additional interstitial oxygen ($La_{8+x}Sr_{2-x}M_6O_{26+x/2}$ (M = Si, Ge; $x>0$), implies that the process of nitridation is driven by the removal of these interstitial anions to yield an overall anion content (N+O) of 26. While $La_{9.33}Si_6O_{26}$ was shown through neutron diffraction studies to accommodate some nitrogen in the SiO_4 tetrahedra and in the oxide anion channels in high temperature reactions with ammonia (>950 °C), the investigation of the strontium doped apatites suggested that this is not a favourable process. In these cases the overall oxygen content does not drop below 24, the minimum required to maintain the $(SiO_4)_6$ tetrahedra [10]. In this paper, we extend this earlier work on heat treatment of apatite electrolytes in NH_3 to transition metal (Co) doped systems, $La_{9.67}Si_5CoO_{26}$, and $La_{10}(Si/Ge)_5CoO_{26.5}$ to examine what effect the presence of a transition metal dopant has on the stability. The presence of a transition metal introduces another variable parameter as, two processes could occur at high temperatures in NH_3; partial substitution of oxide anions with nitride anions in a 3:2 ratio and reduction of the Co induced by the reducing atmosphere created by ammonia. Furthermore, apatite silicates and germanates with and without oxygen hyperstoichiometry have been chosen. In order to determine the relevant processes occurring and the structural stability of the potential electrolytes $La_{9.67}Si_5CoO_{26}$, and $La_{10}(Si/Ge)_5CoO_{26.5}$ when in contact with ammonia at high temperature, the samples have been examined by a combination of X-ray diffraction, extended X-ray absorption fine structure (EXAFS), X-ray absorption near edge structure (XANES) and thermogravimetric analysis.

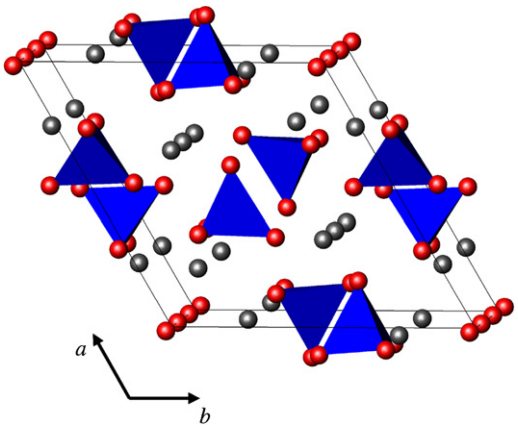

Fig. 1. The apatite structure, $A_{10}(MO_4)_6X_2$. The grey and red spheres represent *A* and O/*X*, respectively. The blue polyhedra are MO_4 tetrahedra. (For interpretation of the references to color in this figure legend, the reader is referred to the web version of this article.)

2. Experimental

$La_{9.67}Si_5CoO_{26}$ and $La_{10}Si_5CoO_{26.5}$ were prepared via the solid state reaction of intimately ground stoichiometric mixtures of La_2O_3, SiO_2 and Co_3O_4 heated twice at 1100 °C and three times at 1300 °C for 12 h with intermediate regrinding. $La_{10}Ge_5CoO_{26.5}$ was prepared via a low temperature Pechini-type sol gel route. Stoichiometric amounts of $La(NO_3)_3\cdot 6H_2O$, GeO_2, and $Co(NO_3)_2\cdot 6H_2O$ were dissolved in water by heating. Once dissolved, citric acid and ethylene glycol were added (1.7 moles per mole of La+Y), and the mixture evaporated on a hot plate until a clear gel was obtained. The gel was then transferred to a furnace and heated at 2 °C/min to 800 °C before holding at this temperature for 12 h, followed by regrinding and reheating to 950 °C for a further 12 h.

Silicon containing samples were heated in flowing ammonia (233.33 cm^3/min) at 800 and 1000 °C for 12 h, while the germanium containing samples were heated for 12 h at the lower temperatures of 600 and 800 °C. A lower temperature was used for the latter; as previous work had indicated that nitridation occurred at lower temperatures in germanate apatites [11].

Powder X-Ray diffraction (PXRD) was performed using a Siemens D5000 powder diffractometer with Cu $K\alpha$ radiation (current=30 mA, voltage=40 kV, step size=0.019°, step size=2 s, Ge(1 1 1) primary beam monochromator). The nitrogen contents of the samples after heat treatment in ammonia were determined through thermogravimetric analysis with a Netzsch STA 449 thermal analyser in the range of temperature 25–1000 °C with ramp rate of 10 °C/min.

EXAFS and XANES measurements were performed at Station 9.3 of the Daresbury Synchrotron Radiation Source operating at 2 GeV with circulating currents of 100–250 mA. The Co–K-edge wavelengths were selected using a Si(1 1 1) double crystal monochromator, and harmonic rejection used a Pd-coated mirror. The apatite samples were diluted in boron nitride and the data collected in fluorescence mode at room temperature. The Co standards were collected in transmission mode, again at room temperature. $CoCr_2O_4$, $YSr_2Cu_2CoO_7$ and $LaCoO_3$ were prepared by solid state reaction, while [Co(salen)]$_2$ [bis(μ_2-(bis(salicylaldehyde)-ethylenediiminato-N,N′,O,O,O′)-cobalt(II))], [Co(acac)$_2$.H_2O]$_2$ [bis(aqua-(μ_2-acetylacetonato-O,O,O′)-(acetylacetonato)-cobalt(II))] were obtained from Aldrich and used as supplied. Co3,5-^{t}Bu-Cysalen [((R,R)-(-)-N,N′-bis(3,5-Di-t-butylsalicylidene)-1,2-cyclohexanediamino)cobalt(II)] was prepared by Woodward's group at the University of Nottingham [17].

The spectra were calibrated using the first maximum in the first derivative of Co foil (7709.0 eV), and this was monitored with a Co foil placed between second and third ion chambers.

Averaging and calibration (using monochromator position) of the spectra was achieved within PAXAS, [18] and background subtraction employed PySpline [19]. The pre-edge peak positions were taken as the maximum of the peak/crossing point in the first derivative, whereas the edge position was taken as the maximum of the first derivative in the edge region. The data were fitted using curved wave, single scattering theory within EXCURV98 [20]. The quality of fit is indicated by an *R*-factor, but the statistical significance of including additional shells made use of the reduced χ^2 function within EXCURV98.

3. Results and discussion

3.1. Powder X-ray diffraction (PXRD)

Comparison of PXRD patterns of starting and ammoniated $La_{9.67}Si_5CoO_{26}$, $La_{10}Si_5CoO_{26.5}$, $La_{10}Ge_5CoO_{26.5}$ samples are shown in Figs. 2–4. No impurity peaks are detected in the PXRD patterns

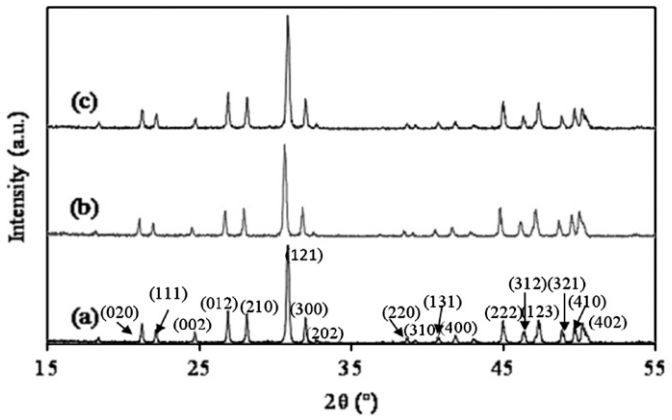

Fig. 2. PXRD patterns for $La_{9.67}Si_5CoO_{26}$ (a), after reaction in NH_3 at 800 °C (b) and after reaction in NH_3 at 1000 °C (c).

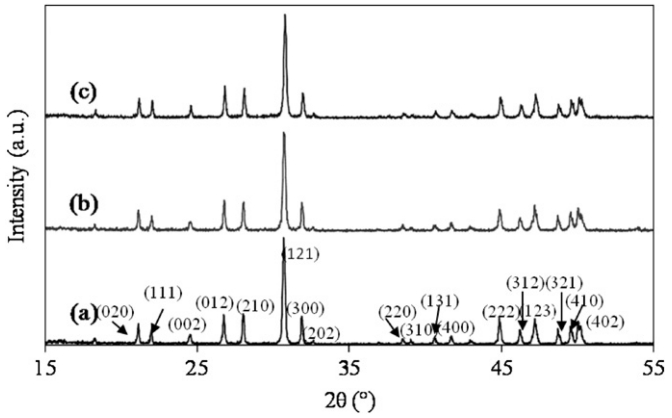

Fig. 3. PXRD patterns for $La_{10}Si_5CoO_{26.5}$ (a), after reaction in NH_3 at 800 °C (b) and after reaction in NH_3 at 1000 °C (c).

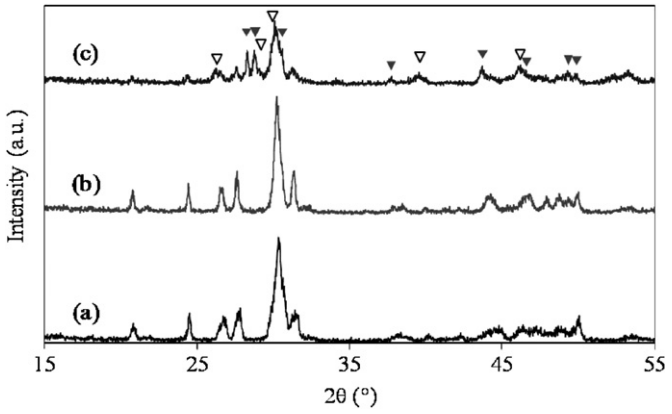

Fig. 4. PXRD patterns for $La_{10}Ge_5CoO_{26.5}$ (a), after reaction in NH_3 at 600 °C (b) and after reaction in NH_3 at 800 °C (c). The solid and clear triangles indicate the main peaks for La_2O_3 and La_4GeO_8, respectively.

after ammoniation for $La_{9.67}Si_5CoO_{26}$ and $La_{10}Si_5CoO_{26.5}$ at all reaction temperatures investigated, showing that the apatite structure is maintained at elevated temperatures in the presence of this fuel. In contrast, $La_{10}Ge_5CoO_{26.5}$ showed evidence of partial decomposition after reaction with ammonia at 800 °C with the occurrence of impurities such as La_4GeO_8 and La_2O_3 (Fig. 4).

The PXRD patterns of the silicate samples were indexed to a hexagonal unit cell ($P6_3/m$, $a=b=9.7963(6)$, $c=7.2304(3)$) [21] and the lattice parameters are given in Table 1. The differences in lattice parameters between the starting compounds and the oxide–nitrides are small. It was not possible to calculate the cell parameters of the germanate samples due to the broadness of the diffraction peaks, attributed to a triclinic distortion, which is common in apatite-type germanate systems [16,22,23].

Table 1
Cell parameters for the $La_{9.67}Si_5CoO_{26}$ and $La_{10}Si_5CoO_{26.5}$ samples derived from PXRD at room temperature.

Silicates	*a* (Å)	*c* (Å)
$La_{9.67}Si_5CoO_{26}$	9.7153(7)	7.2369(6)
Ammoniation conditions		
$La_{9.67}Si_5CoO_{26}+NH_3$ 800 °C	9.7359(7)	7.2611(6)
$La_{9.67}Si_5CoO_{26}+NH_3$ 1000 °C	9.7376(10)	7.2639(9)
$La_{10}Si_5CoO_{26.5}$	9.7304(7)	7.2555(7)
Ammoniation conditions		
$La_{10}Si_5CoO_{26.5}+NH_3$ 800 °C	9.7307(10)	7.2619(9)
$La_{10}Si_5CoO_{26.5}+NH_3$ 1000 °C	9.7282(7)	7.2583(7)

3.2. X-ray absorption fine structure spectroscopy

Co K-edge XAFS spectroscopy was carried out in order to determine the coordination environment and oxidation number of cobalt in $La_{9.67}Si_5CoO_{26}$ and $La_{10}M_5CoO_{26.5}$ (M=Si, Ge) oxides and the corresponding ammoniated compounds (oxide–nitrides).

There have been reports that cobalt is an ambi-site dopant, capable of substituting onto either the La or Si/Ge site depending on the starting composition, hence the need for Co standards with different coordination numbers to confirm the substitution site [24].

3.3. Co K-edge XANES of $La_{9.67}Si_5CoO_{26}$ and $La_{10}M_5CoO_{26.5}$ (M=Si, Ge)

Co K-edge XANES is able to provide information about both the oxidation state and coordination environment of the cobalt in the starting materials as well as the products after ammoniation, even for poorly crystallised or amorphous samples. In order to identify the characteristic spectral motifs of cobalt in different coordination geometries and oxidation states a number of standards were studied and their spectra are shown in Fig. 5. $CoCr_2O_4$ (Fig. 5(a)), Co-3,5-*t*-Bu-cysalen (Fig. 5(b)), $[Co(salen)]_2$ (Fig. 5(c)) and $[Co(acac)_2\cdot H_2O]_2$, (Fig. 5(d)) display Co^{2+} in tetrahedral, square planar, square-based pyramidal and octahedral coordination, respectively [25,26]. $LaCoO_3$ (Fig. 5(e)), $YSr_2Cu_2CoO_7$ (Fig. 5(f)) contain Co^{3+} in octahedral and tetrahedral coordination, respectively [27,28]. From both the spectra and first derivatives of $CoCr_2O_4$ (Fig. 5(a)) and $YSr_2Cu_2CoO_7$ (Fig. 5(e)) it can be seen that on going from tetrahedral Co^{2+} to Co^{3+} there is a shift to higher energy of 4.3 eV for the edge and 1.3 eV for the pre-edge feature. For the octahedral examples, $[Co(acac)_2H_2O]_2$ (Fig. 5(d)) and $LaCoO_3$ (Fig. 5(e)), there is a shift of 2.9 eV for edges, but with very weak pre-edge feature. In addition to the characteristic edge positions of the different oxidation states, Fig. 5 also shows that the Co K-edge XANES structure is very dependent on the coordination environment.

The weak features just before the edge, which are associated with 1*s*–3*d* transitions, as well as the features on the edge, which can be thought of as 1*s*–4*p* transitions, are very characteristic of the site symmetry of the Co environment. The intensity of the 1*s*–3*d* pre-edge features is very dependent on the symmetry of the Co environment, and in particular the presence of a centre of

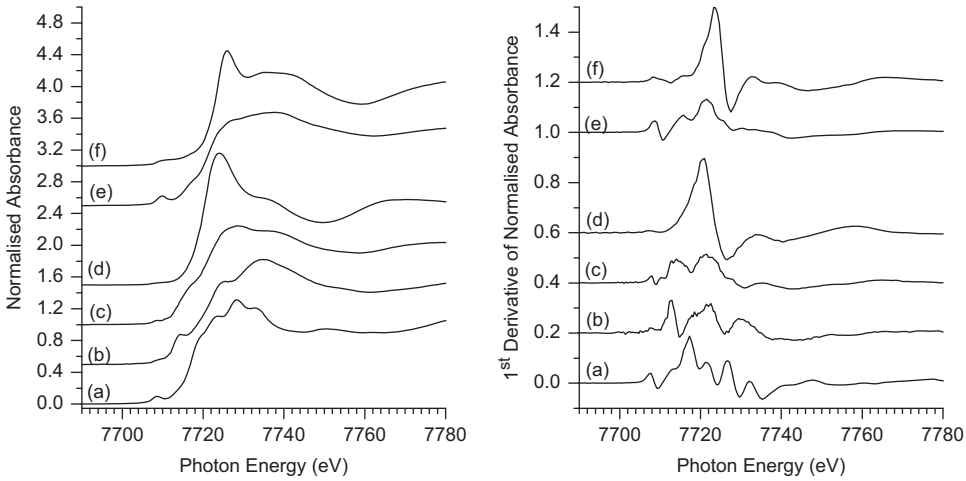

Fig. 5. Co K-edge XANES (left) and first derivative (right) spectra of (a) $CoCr_2O_4$, (b) Co-3,5-^{t}Bu-cysalen, (c) $[Co(salen)]_2$, (d) $[Co(acac)_2H_2O]_2$, (e) $YSr_2Cu_2CoO_7$ and (f) $LaCoO_3$.

Table 2
Co K-edge positions for oxides, ammoniated oxides and standards.

Compound/reaction conditions	Pre-edge position (eV)	Edge position (eV)
$La_{9.67}Si_5CoO_{26}$	7709.6	7720.6
$La_{10}Si_5CoO_{26.5}$	7709.7	7720.4
$La_{10}Ge_5CoO_{26.5}$	7709.8	7720.5
$La_{9.67}Si_5CoO_{26}+NH_3$ 800 °C	7708.7	7718.8
$La_{10}Si_5CoO_{26.5}+NH_3$ 800 °C	7708.6	7718.5
$La_{10}Ge_5CoO_{26.5}+NH_3$ 600 °C	7709.1	7718.6
$La_{9.67}Si_5CoO_{26}+NH_3$ 1000 °C		7708.5
$La_{10}Si_5CoO_{26.5}+NH_3$ 1000 °C		7708.0
$La_{10}Ge_5CoO_{26.5}+NH_3$ 800 °C		7708.0
$CoCr_2O_4$	7708.6	7717.2
Cocysalen	7714.4	7722.0
$[Co(salen)]_2$	7708.5	7714.0
$[Co(acac)_2H_2O]_2$	7708.9	7720.6
$YSr_2Cu_2CoO_7$	7709.9	7721.5
$LaCoO_3$	7712.0	7723.5
Co metal		7709.0

symmetry and/or extensive p–d mixing of the 3d orbitals. In the spectra of octahedral $[Co(acac)_2\cdot H_2O]_2$ (Fig. 5(d)) and square-planar (Co-3,5-^{t}Bu-cysalen (Fig. 5(b)) the 1s–3d transitions are very weak. In the spectra of square-based pyramidal $[Co(salen)]_2$ (Fig. 5(c)) the pre-edge feature has increased intensity and in the spectra of tetrahedral $CoCr_2O_4$ (Fig. 5(a)) the 1s–3d transitions has greater intensity. The presence of well-defined shoulders on the edge itself has been assigned previously to 1s–4p_z transitions (with shakedown contributions) in tetragonal geometries where one or more axial ligands are absent [28–30]. For square-planar Co-3,5-^{t}Bu-cysalen (Fig. 5(b)), this shoulder is more marked than for square-based pyramidal $[Co(salen)]_2$ (Fig. 5(c)). A similar picture emerges for the Co^{3+} spectra where a more intense pre-edge feature is observed for tetrahedral $YSr_2Cu_2CoO_7$, but which is absent in the spectra of octahedral $LaCoO_3$. The position of the pre-edge features and edge positions are collected together in Table 2. Therefore, Co K-edge XANES spectra were recorded on both the starting apatite samples, and after ammoniation to identify the cobalt oxidation states and coordination environments.

The Co–K-edge XANES spectrum of $La_{9.67}Si_5CoO_{26}$ has been investigated previously by Tolchard et al. and the oxidation state and coordination of the cobalt was confirmed to be 3+ in tetrahedral coordination to four oxide anions [24]. The same Co^{3+} oxidation state and geometry is predicted for cobalt in $La_{10}Si_5CoO_{26.5}$ and $La_{10}Ge_5CoO_{26.5}$, from simple charge balancing considerations. The spectra of the silicates and germanates are compared in Fig. 6, together with appropriate standards. The spectra and first derivatives of $La_{9.67}Si_5CoO_{26}$ (Fig. 6(a)), $La_{10}Si_5CoO_{26.5}$ (Fig. 6(b)) and $La_{10}Ge_5CoO_{26.5}$ (Fig. 6(c)) are all essentially identical indicating that the oxidation states and coordination geometries are the same in all three. The presence of a relatively intense pre-edge feature at ca. 7709.7 compared to 7709.9 eV for $YSr_2Cu_2CoO_7$ (Fig. 6(d)) indicates the presence of tetrahedral Co^{3+}. There is also a striking similarity between both the spectra and the first derivatives of the apatite samples (Fig. 6(a–c) and that of $YSr_2Cu_2CoO_7$ (Fig. 6(d)). The spectrum of octahedral $LaCoO_3$ (Fig. 6(e)) is very different with only a very weak pre-edge and completely different edge structure. Therefore, the Co K-edge XANES data confirms the presence of Co^{3+} tetrahedrally coordinated by O^{2-} anions in all of the apatite samples.

These data also confirm that Co^{3+} is substituting for Si^{4+}/Ge^{4+} and not La^{3+}, for which computer modelling studies suggest reduction from a ninefold to a sixfold coordination when partially substituted by a smaller dopant [31].

3.4. Co K-edge XANES of ammoniated $La_{9.67}Si_5CoO_{26}$, $La_{10}M_5CoO_{26.5}$ (M=Si, Ge)

Fig. 7 shows the Co K-edge XANES spectra of $La_{10}Si_5CoO_{26.5}$ before (Fig. 7(b)) and after (Fig. 7(c)) reaction with ammonia at 800 °C, together with $YSr_2Cu_2CoO_7$ (Fig. 7(a)) and $CoCr_2O_4$ (Fig. 7(d)). It is clear that on reaction with ammonia, the pre-edge feature is retained with similar intensity, but shifted to lower energy, indicating that tetrahedral coordination of the Co is still present. The shift in edge position due to the reaction with ammonia is 1.9 eV to lower energy and this should be compared to a shift of 4.3 eV observed between the spectra of $YSr_2Cu_2CoO_7$ (Fig. 7(a)) and $CoCr_2O_4$ (Fig. 7(d)). The pre-edge peak shifts by 0.7 eV compared to 1.3 eV for $YSr_2Cu_2CoO_7$ and $CoCr_2O_4$. Therefore, the Co K-edge XANES spectra indicate that reaction of $La_{10}Si_5CoO_{26.5}$ with ammonia at 800 °C, results in the reduction of Co^{3+} to Co^{2+}, but that the reduction is probably not complete. The tetrahedral coordination environment is maintained.

The behaviour of $La_{10}Ge_5CoO_{26.5}$ (Fig. 8(b)) after reaction with ammonia at 600 °C (Fig. 8(c)) was very similar to that observed for $La_{10}Si_5CoO_{26.5}$ with a shift of 0.7 eV in the pre-edge peak and 1.9 eV in the edge position again indicating partial reduction to Co^{2+}. The spectra of $La_{9.67}Si_5CoO_{26}$ before (Fig. 9 (a)) and after

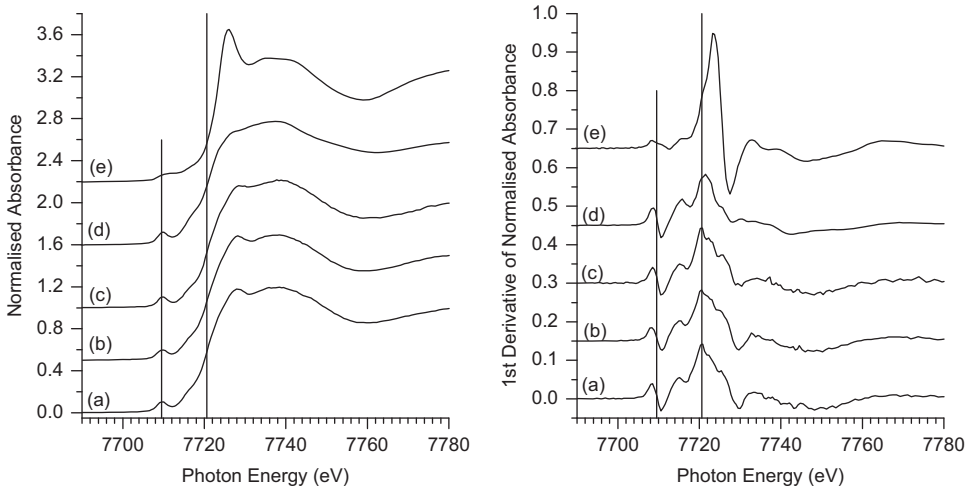

Fig. 6. Co K-edge XANES (left) and first derivative (right) spectra of (a) $La_{9.67}Si_5CoO_{26}$, (b) $La_{10}Si_5CoO_{26.5}$, (c) $La_{10}Ge_5CoO_{26.5}$, (d) $YSr_2Cu_2CoO_7$ and (e) $LaCoO_3$. Vertical markers are at 7709.5 and 7720.6 eV.

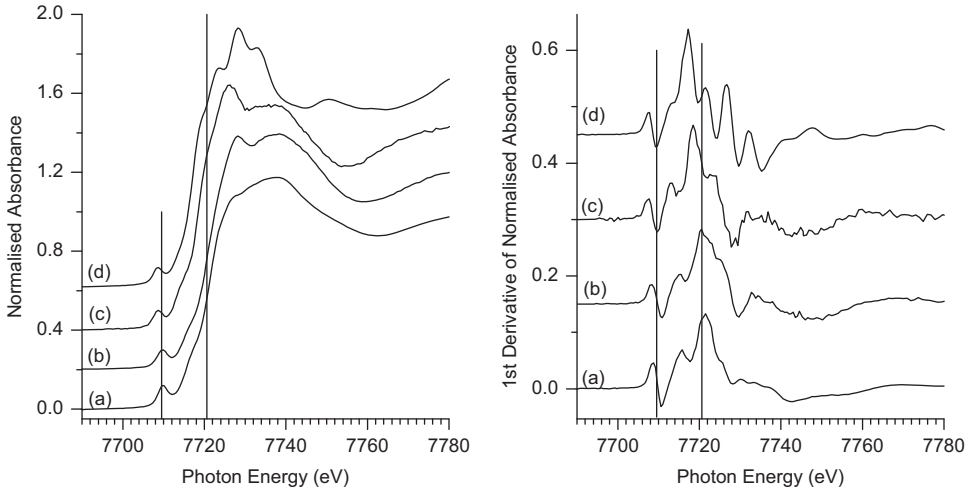

Fig. 7. Co K-edge XANES (left) and first derivative (right) spectra of (a) $YSr_2Cu_2CoO_7$, (b) $La_{10}Si_5CoO_{26.5}$, (c) $La_{10}Si_5CoO_{26.5}$ after ammonolysis at 800 °C and (d) $CoCr_2O_4$. Vertical markers are at 7709.5 and 7720.6 eV.

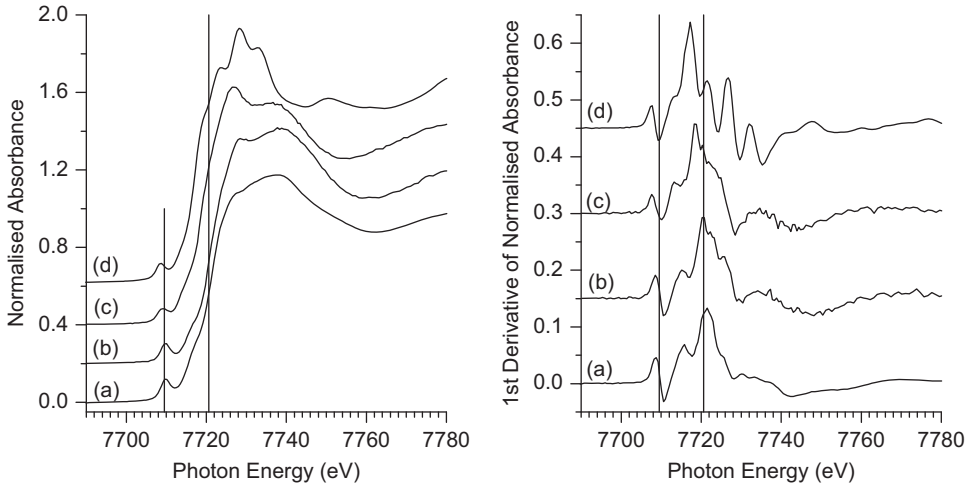

Fig. 8. Co K-edge XANES (left) and first derivative (right) spectra of (a) $YSr_2Cu_2CoO_7$, (b) $La_{10}Ge_5CoO_{26.5}$, (c) $La_{10}Ge_5CoO_{26.5}$ after ammonolysis at 600 °C and (d) $CoCr_2O_4$. Vertical markers are at 7709.5 and 7720.6 eV.

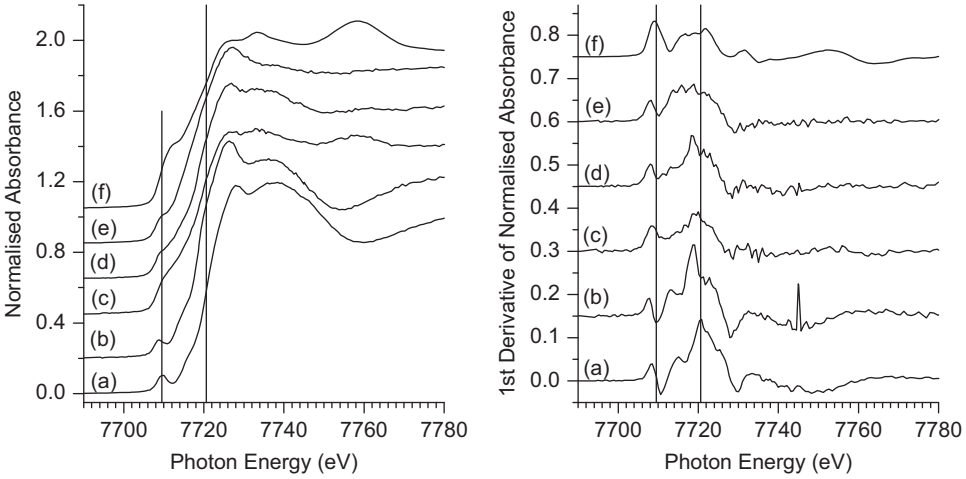

Fig. 9. Co K-edge XANES (left) and first derivative (right) spectra of (a) $La_{9.67}Si_5CoO_{26}$, (b) $La_{9.67}Si_5CoO_{26}$ after ammonolysis at 800 °C, (c) $La_{9.67}Si_5CoO_{26}$ after ammonolysis at 1000 °C (d) $La_{10}Si_5CoO_{26.5}$ after ammonolysis at 1000 °C, (e) $La_{10}Ge_5CoO_{26.5}$ after ammonolysis at 800 °C and (f) Co metal foil. Vertical markers are at 7709.5 and 7720.6 eV.

reaction with ammonia at 800 °C (Fig. 9(b)) were essentially identical to those of $La_{10}Si_5CoO_{26.5}$ (Fig. 7(b,c)) under the same conditions with shifts of 0.9 eV of the pre-edge peak and 1.8 eV of the edge.

When the reaction temperature was increased to 1000 °C for the silicates and 800 °C for the germanates, the characteristic pre-edge feature is lost under a new edge feature, and this is most marked for $La_{9.67}Si_5CoO_{26}$ (Fig. 9(c)), although this also occurs for $La_{10}Si_5CoO_{26.5}$ (Fig. 9(d)) and $La_{10}Ge_5CoO_{26.5}$ (Fig. 9(e)). Whilst the loss of intensity of the pre-edge peak can be attributed to the cobalt being in an octahedral or square planar environment, in this case the XANES spectrum and first derivative of $La_{9.67}Si_5CoO_{26}$ (Fig. 9(c)) are very similar to that of cobalt metal (Fig. 9(f)) and therefore it appears that on heating $La_{9.67}Si_5CoO_{26}$ above 800 °C further reduction of the cobalt results in the formation of metallic cobalt. For $La_{10}Si_5CoO_{26.5}$ (Fig. 9(d)) and $La_{10}Ge_5CoO_{26.5}$ (Fig. 9(e)) the Co K-edge XANES spectra have features characteristic of metallic cobalt, but the edge structure indicates that the reduction is not so advanced as for $La_{9.67}Si_5CoO_{26}$. These data indicate that the combination of the reducing atmosphere and higher temperature cause partial decomposition of the apatite structure via loss of cobalt in its metallic form. The cobalt metal is probably present in an amorphous form as no diffraction peaks are present in the PXRD patterns (Figs. 2–4). Further evidence for this presence of Co metal is shown in the EXAFS spectra in the following section. A summary of all Co K-edge positions for all Co-containing apatites, the ammoniated compounds and the standards is provided in Table 2.

3.5. Co K-edge EXAFS of $La_{9.67}Si_5CoO_{26}$, $La_{10}M_5CoO_{26.5}$ (M=Si, Ge)

As the Co K-edge XANES spectra indicated a tetrahedral environment of Co^{3+} for the three starting materials, $La_{9.67}Si_5CoO_{26}$, $La_{10}Si_5CoO_{26.5}$ and $La_{10}Si_5GeO_{26.5}$ the EXAFS spectra were analysed assuming a coordination environment of four oxide anions to model the first shell. Previous modelling of the data for $La_{9.66}Si_5CoO_{26}$ had been limited to the first shell as including further shells proved difficult [24].

The Co K-edge EXAFS and FT from $La_{9.67}Si_5CoO_{26}$ are shown in Fig. 10(a). Initially, the Co–O interaction was Fourier filtered to isolate this from other features. The Co–O bond length of 1.84(2) Å is consistent with 1.85(2) Å previously obtained from EXAFS analysis by Tolchard et al. [24] and with literature values of Co–O bond lengths in tetrahedral coordination, i.e. ~1.905 Å in $YSr_2Cu_2Co(III)O_7$ and ~1.986 Å in $Co(II)Cr_2O_4$ [24,27,28]. The EXAFS Co–O bond length which targets the cobalt site exclusively is significantly longer than that found by neutron diffraction (~ 1.65 Å) since the latter gives an average (Si/Co)-O bond length. [24].

Having fitted the first shell, attempts were made to model the more distant shells using the original, non-Fourier filtered data in conjunction with the neutron diffraction data as a guide to identify the likely atomic arrangements beyond the first shell [24].

The proposed crystallographic cobalt coordination spheres, beyond the CoO_4 tetrahedra, derived from neutron diffraction are shown in Fig. 11 and the bond lengths within 3.5 Å of the silicon/cobalt centre are given in Table 3 [24].

The larger atoms are more easily identified from the EXAFS data due to their greater scattering cross section and, therefore, lanthanum cations were used to model the remaining absorption intensity in the EXAFS spectra, whilst the oxygen atoms were ignored. The neutron diffraction data shows four lanthanum atoms within 3.5 Å of Si/Co [24]. These consist of two La(3) atoms, which are adjacent to the oxide anion channel and are part of the same $[O(5)La(3)_3]^{7+}$ triangular planar polyhedron, and two La atoms which lie between the $(Si/Co)O_4$ tetrahedra, La(1) and La(2). La(1) and La(2) alternate in linear chains running parallel to the *c*-axis. The lanthanum cations can be separated into two shells, one lanthanum at 3.271 Å (La(3)) and three lanthanum atoms at 3.340 Å, from cobalt [23]. Refinement of these parameters demonstrated a statistically significant improvement in the fit when two Co–La shells were used rather than just one. The EXAFS and Fourier transformations for $La_{9.67}Si_5CoO_{26}$ are shown in Fig. 10(a) and the structural parameters obtained from the fitting of the data are shown in Table 4.

The Co–La interatomic distances derived from EXAFS indicate a small reduction in all values compared to those found by neutron diffraction, but remain consistent with the apatite structure (Table 4).

The same data analysis procedure was applied to the EXAFS data for $La_{10}Si_5CoO_{26.5}$ and $La_{10}Ge_5CoO_{26.5}$ and their EXAFS and FTs are shown in Fig. 10(b) and (c), respectively. The refined structural parameters are given in Table 5.

The Co–O and Co–La interatomic distances for $La_{10}Si_5CoO_{26.5}$ are effectively identical to those derived from the EXAFS of $La_{9.67}Si_5CoO_{26}$, indicating that the Co coordination environment is

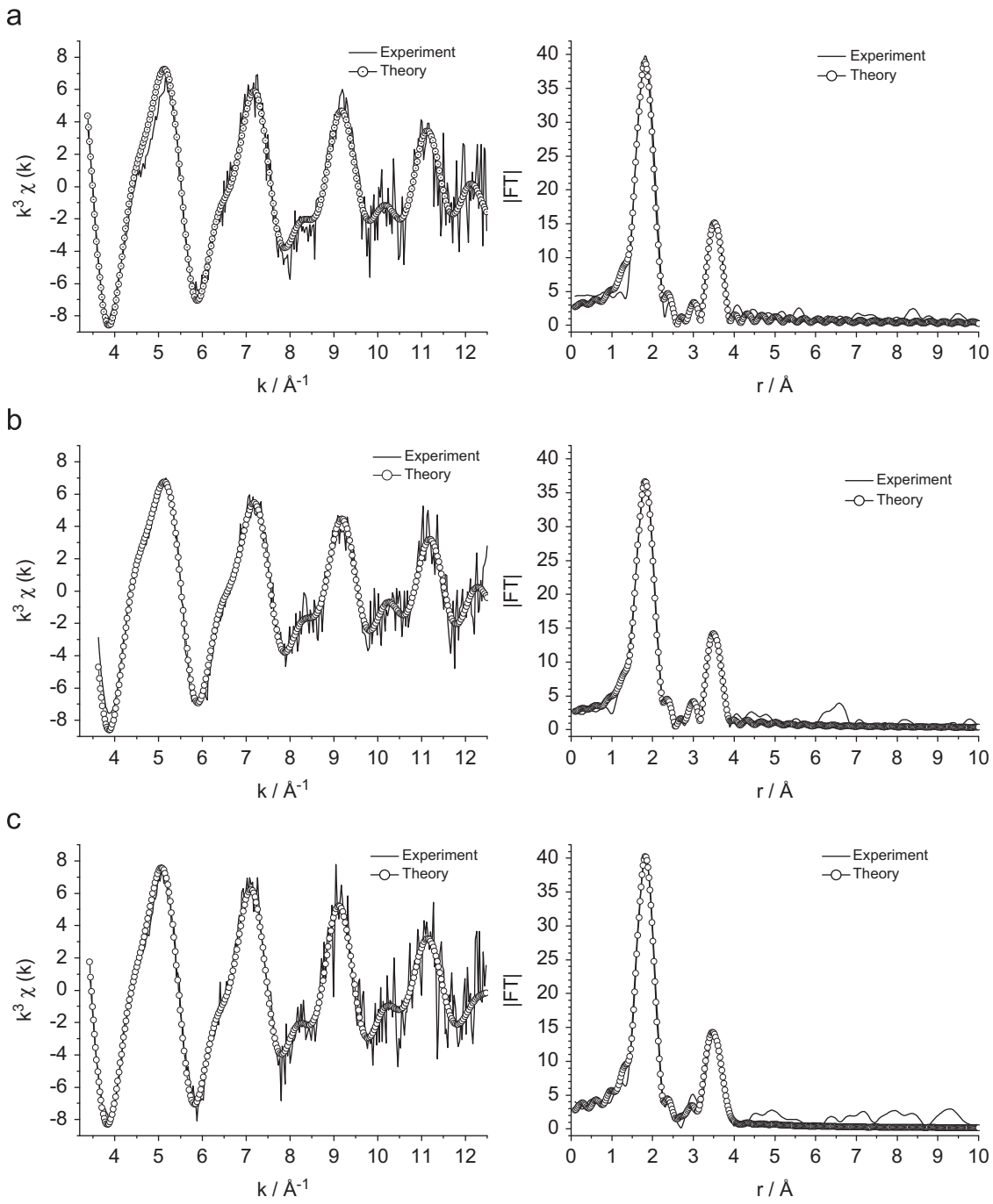

Fig. 10. Co K-edge EXAFS (left) and FT (right) for (a) $La_{9.67}Si_5CoO_{26}$, (b) $La_{10}Si_5CoO_{26.5}$ and (c) $La_{10}Ge_5CoO_{26.5}$.

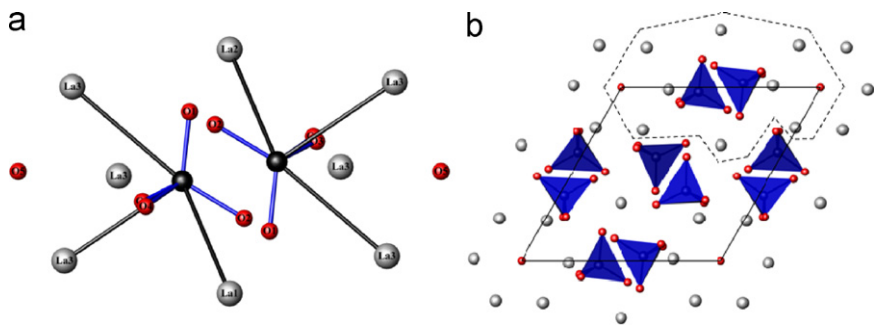

Fig. 11. (a) The silicon/cobalt coordination (bond lengths <3.5 Å) in $La_{9.66}Si_5CoO_{26.5}$, deduced from neutron diffraction. (b) The Si/Co coordination is highlighted, by the dotted line, in relation to the whole structure.

the same in both. The results therefore would suggest that there is no strong preference for the interstitial site to be neighbouring Co (i.e. no strong dopant-interstitial interactions), which is consistent with the reported high conductivities of these phases. [16].

The EXAFS and Fourier transformations for $La_{10}Ge_5CoO_{26.5}$ are shown in Fig. 10(c) and the structural parameters obtained from the fitting of the data are given in Table 5. Whilst the data quality meant that it was only possible to model two shells (Co–O and Co–La), with the single Co–La(3) shell omitted, the data do indicate that the Co environment is similar to that for the silicates.

In general, the EXAFS analysis indicates that $La_{10}Ge_5CoO_{26.5}$ demonstrates similar structural features as the silicate counterparts. It does, however, appear that the Co–O bond length in $La_{10}Ge_5CoO_{26.5}$ is slightly longer than those observed in $La_{9.67}Si_5CoO_{26}$ and $La_{10}Si_5CoO_{26.5}$. The Debye–Waller factors of all samples are similar, so the difference in bond length is not attributed to increased tetrahedral distortion.

Table 3
Selected bond lengths in $La_{9.66}Si_5CoO_{26.5}$ derived from neutron diffraction data [24].

Bond lengths (Å)			
Si/Co–O(1)	1.607	Si/Co–La(3)	3.271
Si/Co–O(2)	1.664	Si/Co–La(2)	3.323
	3.213	Si/Co–La(3)	3.336
Si/Co–O(3)	1.590	Si/Co–La(1)	3.360
Si/Co–O(4)	1.734		

3.6. Co K-edge EXAFS of ammoniated $La_{9.67}Si_5CoO_{26}$, $La_{10}M_5CoO_{26.5}$ (M=Si, Ge)

Ammonolysis of the apatite materials, $La_{9.67}Si_5CoO_{26}$ and $La_{10}Si_5CoO_{26.5}$ at 800 °C and $La_{10}Ge_5CoO_{26.5}$ at 600 °C, has been confirmed through XANES and PXRD to cause no overall deterioration in the apatite structure. TGA, shown in the following section indicates that all samples also show a reduction in oxygen content, while nitrogen has been incorporated into the oxygen hyperstoichiometric $La_{10}M_5CoO_{26.5}$ (M=Si, Ge) samples only. The latter observation is consistent with prior studies of non-transition metal doped systems, where the level of nitridation increased with increasing interstitial oxygen content [11]. The three proposed stoichiometries, calculated from TGA data, are $La_{9.67}Si_5CoO_{25.62}$, $La_{10}Si_5CoO_{25.87}N_{0.18}$ and $La_{10}Ge_5CoO_{26.08}N_{0.13}$. These imply average cobalt oxidation states of $Co^{2.23+}$, $Co^{2.28+}$ and $Co^{2.55+}$, indicating a mixed Co^{2+}/Co^{3+} state, in good agreement

Table 4
Summary of refined Co K-edge EXAFS parameters for $La_{9.67}Si_5CoO_{26}$, $La_{10}Si_5CoO_{26.5}$ and $La_{10}Ge_5CoO_{26.5}$.

Shell	Atom type	Coordination	r (Å)[a,b]	D–W factor (Å^2)[a,c]	E_f (eV)[a,d]	R-fit (%)[e]
$La_{9.67}Si_5CoO_{26}$					−1.9(6)	28.87
1	O^{2-}	4	1.854(5)	0.011(1)		
2	La^{3+}	1	3.113(18)	0.010(3)		
3	La^{3+}	3	3.277(11)	0.014(2)		
$La_{10}Si_5CoO_{26.5}$					−1.5(4)	24.89
1	O^{2-}	4	1.857(5)	0.012(1)		
2	La^{3+}	1	3.096(22)	0.015(5)		
3	La^{3+}	3	3.264(10)	0.016(2)		
$La_{10}Ge_5CoO_{26}$					−3.2(9)	24.89
1	O^{2-}	4	1.866(5)	0.010(1)		
2	La^{3+}	3	3.282(9)	0.020(2)		

[a] Refinement standard deviation in parentheses.
[b] Estimated systematic errors in EXAFS bond lengths are × 1.5% for well-defined co-ordination shells.
[c] D–W is the Debye–Waller factor.
[d] E_f is a single refined parameter to reflect differences in the theoretical and experimental Fermi levels.
[e] $R = [\int |\chi^T - \chi^E| k^3 dk \int |\chi^E| k^3 dk] \times 100\%$.

Table 5
Summary of refined Co K-edge EXAFS parameters for $La_{9.67}Si_5CoO_{26}$ after reaction with NH_3 at 800 °C, $La_{10}Si_5CoO_{26.5}$ after reaction with NH_3 at 800 °C and $La_{10}Ge_5CoO_{26.5}$ after reaction with NH_3 at 600 °C.

Shell	Atom type	Coordination	r (Å)[a,b]	D-W factor (Å^2)[a,c]	E_f (eV)[a,d]	R-fit (%)[e]
$La_{9.67}Si_5CoO_{26}$					−1.1(21)	53.10
1	O^{2-}	4	1.922(10)	0.010(2)		
$La_{10}Si_5CoO_{26.5}$					−3.6(9)	29.67
1	O^{2-}	4	1.918(4)	0.008(1)		
2	La^{3+}	1	3.159(54)	0.016(9)		
3	La^{3+}	3	3.288(23)	0.024(12)		
4	La^{3+}	2	3.577(16)	0.013(3)		
$La_{10}Ge_5CoO_{26}$					−3.2(15)	42.52
1	O^{2-}	4	1.930(7)	0.013(1)		

[a] Refinement standard deviation in parentheses.
[b] Estimated systematic errors in EXAFS bond lengths are × 1.5% for well-defined co-ordination shells.
[c] D–W is the Debye–Waller factor.
[d] E_f is a single refined parameter to reflect differences in the theoretical and experimental Fermi levels.
[e] $R = [\int |\chi^T - \chi^E| k^3 dk \int |\chi^E| k^3 dk] \times 100\%$.

with the XANES data where partial reduction of Co^{3+} was observed.

In the case of $La_{9.67}Si_5CoO_{25.62}$, derived from the reaction of $La_{9.67}Si_5CoO_{26}$ in ammonia at 800 °C, there appears to be only a small reduction in the oxygen stoichiometry and TGA does not indicate any N^{3-} incorporation. The most likely site for the oxide removal is the oxide anion channel as the ability of this site to incorporate anion vacancies was demonstrated in the ammoniation of $La_{9.33}Si_6O_{26}$. This implies the CoO_4 tetrahedra would remain relatively unaltered in $La_{9.67}Si_5CoO_{26}$ after ammonolysis, and this was confirmed by the XANES data. Due to the relatively poor data quality only the first shell could be modelled satisfactorily. The EXAFS and FT for $La_{9.67}Si_5CoO_{25.62}$ are shown in Fig. 12(a) and the structural parameters obtained from the fitting of the data are given in Table 5.

The Co–O bond lengths show a significant increase from 1.85(2) Å in $La_{9.67}Si_5CoO_{26}$, to 1.92(2) Å, in $La_{9.67}Si_5CoO_{25.62}$. The larger cobalt cation radius associated with the lower oxidation state after ammonolysis, confirms the XANES data and compares favourably with the literature values of Co–O bond lengths in tetrahedral coordination, (~1.905 Å in $YSr_2Cu_2Co(III)O_7$ and ~1.986 Å in $Co(II)Cr_2O_4$ [24,27,28]).

Both the $La_{10}M_5CoO_{26.5}$ (M=Si, Ge) samples show only a small degree of N^{3-} incorporation. The total oxygen stoichiometry does

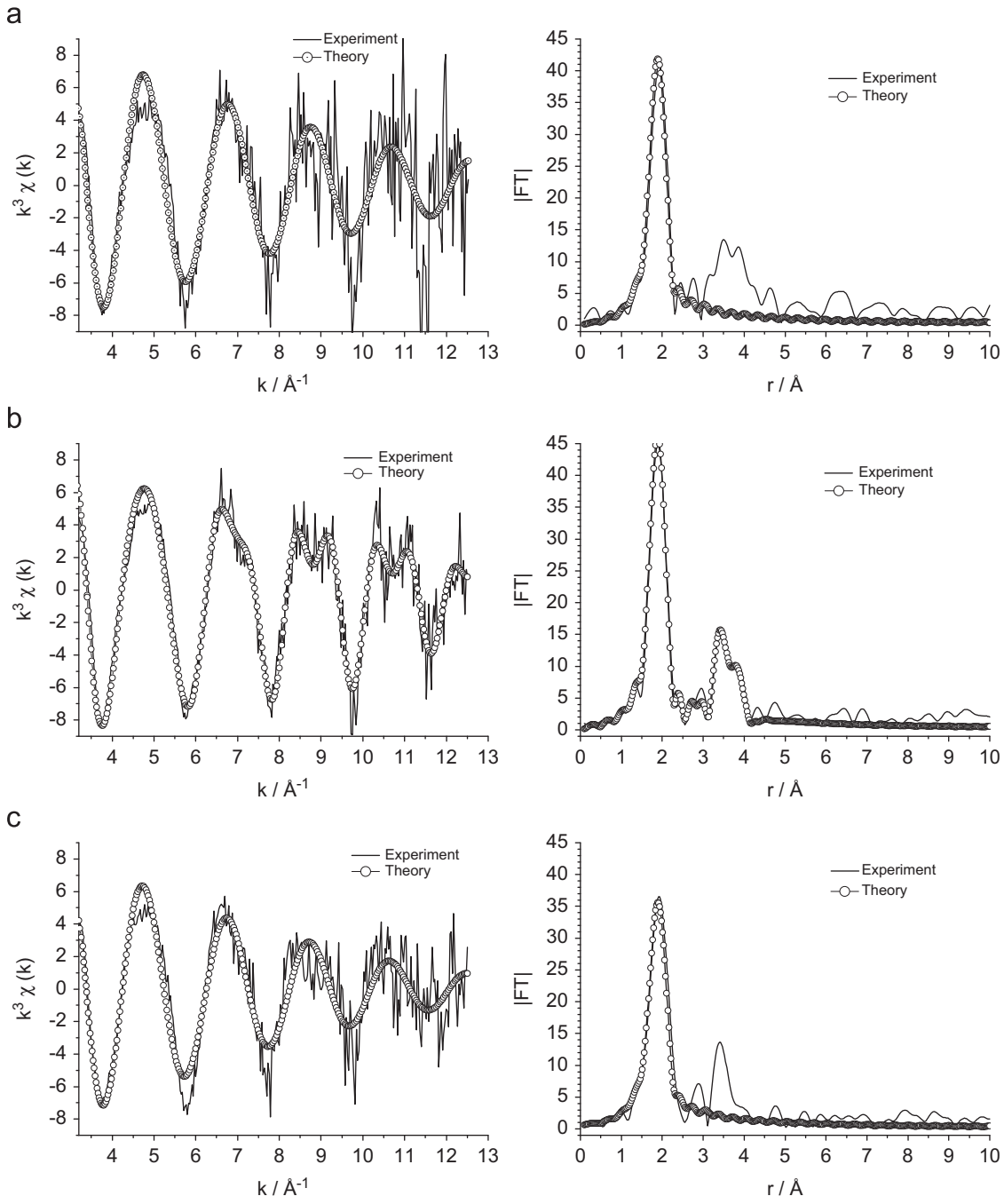

Fig. 12. Co K-edge EXAFS (left) and FT (right) for (a) $La_{9.67}Si_5CoO_{26}$ after reaction in NH_3 at 800 °C, (b) $La_{10}Si_5CoO_{26.5}$ after reaction in NH_3 at 800 °C and (c) $La_{10}Ge_5CoO_{26.5}$ after reaction in NH_3 at 600 °C.

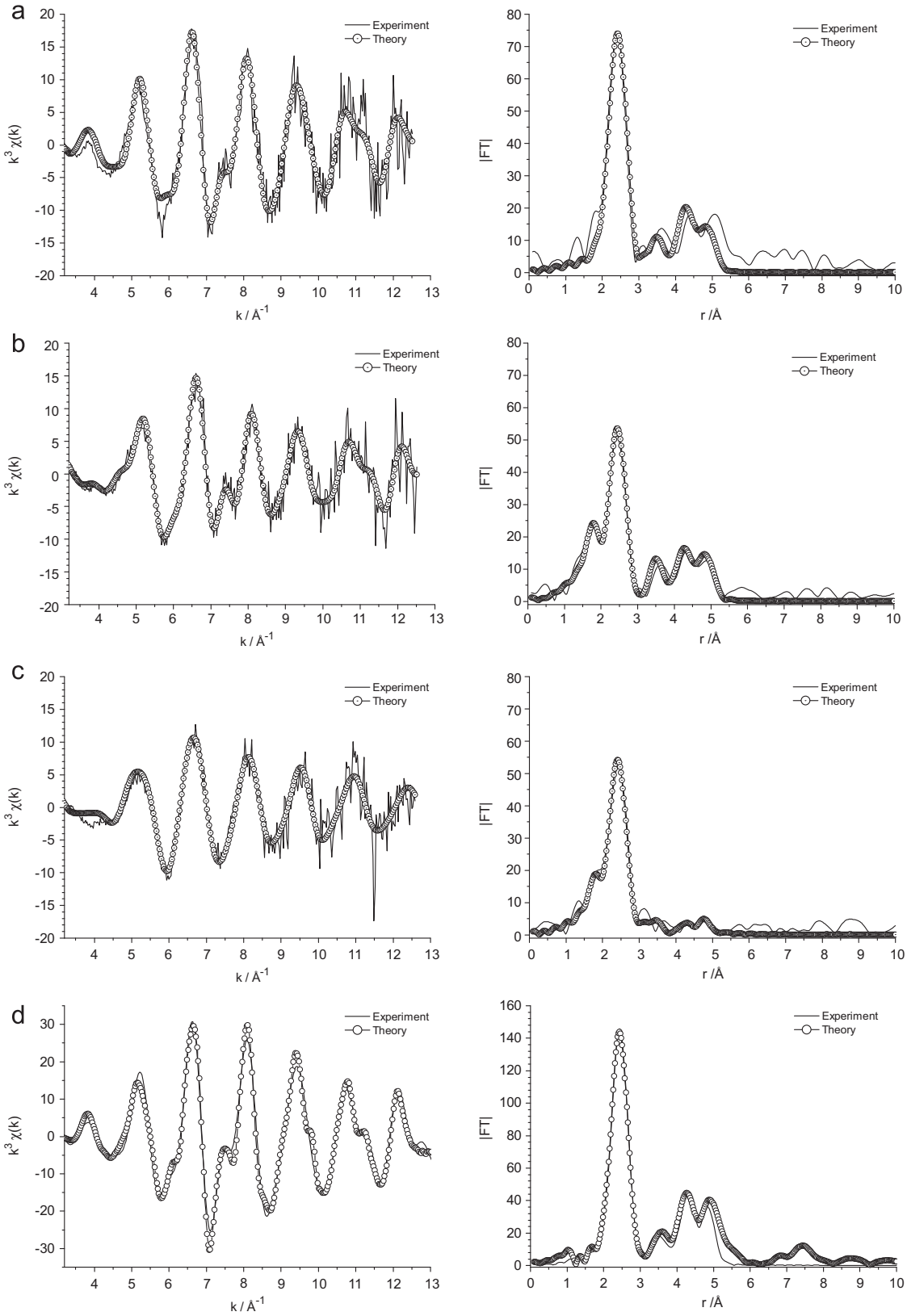

Fig. 13. Co K-edge EXAFS (left) and FTs (right) for (a) $La_{9.66}Si_5CoO_{26}$ after reaction in NH_3 at 1000 °C, (b) $La_{10}Si_5CoO_{26.5}$ after reaction in NH_3 at 1000 °C, (c) $La_{10}Ge_5CoO_{26.5}$ after reaction in NH_3 at 800 °C and (d) Co foil.

not fall below 24, as in $La_{10}Si_5CoO_{25.87}N_{0.18}$ and $La_{10}Ge_5CoO_{26.08}N_{0.13}$, consistent with the MO_4 tetrahedra remaining predominantly free from nitrogen, as proposed previously for non-TM doped systems. [11]

The Co K-edge EXAFS and Fourier transformations for the $La_{10}Si_5CoO_{26.5}$ sample, heated in ammonia at 800 °C ($La_{10}Si_5CoO_{25.87}N_{0.18}$) are shown in Fig. 13. Initially, the data were modelled using parameters derived from the parent apatite.

As for $La_{9.67}Si_5CoO_{26}$ there is an increase of the Co–O bond length from 1.86(2) to 1.92(2) Å, confirming cobalt reduction as indicated by the XANES spectra. The Co–La parameters remain unaltered, relative to the initial apatite, indicating that the incorporation of such a small amount of nitrogen and the removal of the interstitial oxygen anions does not significantly modify the local Co environment. The FT does, however, show an additional peak just below 4 Å not present in the FT of $La_{10}Si_5CoO_{26.5}$. This peak is best fit by an additional shell of two lanthanum cations, La(1) and La(3), at 3.67(4) Å (distances were initially taken from the neutron diffraction data of $La_{9.66}Si_5CoO_{26}$, [24]). This fit is shown in Fig. 12(b) and the refined parameters are given in Table 5.

The EXAFS and FT for $La_{10}Ge_5CoO_{26.5}$, after reaction with ammonia at 600 °C ($La_{10}Ge_5CoO_{26.08}N_{0.13}$) are shown in Fig. 12(c), with the refined structural parameters are given in Table 5.

In a similar way to the ammonolysis of $La_{10}Si_5CoO_{26.5}$, $La_{10}Ge_5CoO_{26.5}$ shows only a small nitrogen incorporation ($La_{10}Ge_5CoO_{26.08}N_{0.13}$) upon ammonolysis and removal of interstitial oxygen. Owing to the data quality it was only possible to fit the first shell satisfactorily, but the increase in Co–O bond length from 1.87(2) to 1.93(2) Å was consistent with the other ammoniated, cobalt containing, apatites.

Finally we report the results from the high temperature ammonolysis reactions at temperature above 800 °C. The XANES analysis performed on the apatites at these temperatures showed the presence of cobalt metal in $La_{9.67}Si_5CoO_{26}$ and probably also in the other two samples. The absence of cobalt metal peaks in the PXRD patterns indicates that the cobalt is probably amorphous. The Co K-edge EXAFS and FTs are shown in Fig. 13 together with those for a cobalt foil.

As the Co K-edge XANES spectrum of $La_{9.66}Si_5CoO_{26}$ after reaction in NH_3 at 1000 °C (Fig. 9(c)) indicated the presence of metallic cobalt, data from the spectrum of a 5 μm cobalt foil (Fig. 13(d)) was analysed first. Cobalt metal shows a hexagonal close packed structure and this structural model was used to fit the EXAFS data [32]. There are six cobalt shells within ca. 5 Å of the absorbing cobalt atom. One of these at 4.07 Å has an occupation number of two, and when this was included in the model, there was no statistical improvement in the quality of the fit, and therefore it was excluded from the final fit. There is also a shell of six cobalt atoms at twice the distance of the first shell (which itself is made up of two components). Whilst this could be modelled using multiple scattering and splitting the first shell, it was decided to exclude this in the final fit so as to be able to compare the same model with all of the data, as the data from the silicates and germanates is too noisy to make its inclusion appropriate. Therefore, the final fit included four cobalt shells as shown in the first column of Table 6. As to be expected the quality of the fit is very good and acts as a calibrant for the extent of amorphous or small particle size effects in the spectra of the silicates and germanates.

The Co K-edge EXAFS and FT of $La_{9.67}Si_5CoO_{26}$ after reaction with NH_3 at 1000 °C (Fig. 13(a)) are very similar to those of cobalt metal, except that the intensity in both has been reduced by about two thirds. Whilst all of the occupation numbers and Debye–Waller factors for the Co shells could be included in the refinement, this would result in a large number of refined parameters. Therefore, in order to reduce the number of refined parameters, the data were modelled by keeping the ratio of cobalt occupation numbers the same as in the bulk (12:6:18:12), but allowing their total contribution to be refined by a single parameter. The fit indicated a value of 63% for this, giving the coordination number shown in Table 6. Whilst there may be signs of residual Co–O at 1.9 Å, when this was incorporated, the fit was not statistically improved, and so it was not included in the final fit. The region around 4–5 Å is not very well reproduced, but bears similarity to that expected for an fcc lattice. An fcc model was attempted, but this resulted in a slightly worse fit. Therefore, the final fit included in Table 6 and Fig. 13(a) only includes an hcp

Table 6
Summary of refined Co K-edge EXAFS parameters for $La_{9.67}Si_5CoO_{26}$ after reaction with NH_3 at 1000°C, $La_{10}Si_5CoO_{26.5}$ after reaction with NH_3 at 1000 °C and $La_{10}Ge_5CoO_{26.5}$ after reaction with NH_3 at 800 °C.

Shell	Atom type	Coordination	r (Å)[a,b]	D-W factor (Å^2) [a,c]	E_f (eV) [a,d]	R-fit (%)[e]
Co foil XRD	Co foil				−2.4(4)	21.4
2.50	Co	12	2.495(2)	0.0134(3)		
3.54	Co	6	3.523(11)	0.0212(26)		
4.34	Co	18	4.357(6)	0.0164(9)		
4.78	Co	12	4.841(6)	0.0104(9)		
$La_{9.67}Si_5CoO_{26}$					−2.3(12)	40.5
1	Co	7.5	2.490(6)	0.0158(18)		
2	Co	3.7	3.523(28)	0.0232(69)		
3	Co	11.2	4.368(17)	0.0206(36)		
4	Co	7.5	4.868(21)	0.0153(43)		
$La_{10}Si_5CoO_{26.5}$					−2.2(10)	36.4
1	O^{2-}	2	1.927(13)	0.0078(44)		
2	Co	6	2.501(6)	0.0176(9)		
3	Co	3	3.554(17)	0.0160(37)		
4	Co	9	4.368(16)	0.0200(30)		
5	Co	6	4.863(13)	0.0117(27)		
$La_{10}Ge_5CoO_{26}$					4.5(12)	40.8
1	O^{2-}	1.4	1.923(19)	0.0084(65)		
2	Co	5.3	2.472(6)	0.0157(8)		
3	Co	2.6	3.473(66)	0.0376(176)		
4	Co	7.9	4.483(57)	0.0353(142)		
5	Co	5.3	4.726(42)	0.0205(80)		

[a] Refinement standard deviation in parentheses.
[b] estimated systematic errors in EXAFS bond lengths are × 1.5% for well-defined co-ordination shells.
[c] D–W is the Debye–Waller factor.
[d] E_f is a single refined parameter to reflect differences in the theoretical and experimental Fermi levels.
[e] $R = [\int |\chi^T - \chi^E| k^3 dk \int |\chi^E| k^3 dk] \times 100\%$.

cobalt environment, but with reduced occupation numbers of 63%. Whilst the reduction in coordination numbers might be indicative of the presence of small (nano)particles, the persistence of more distant shells indicates that the reduction in coordination number is much more likely to be due to the cobalt being amorphous together with a small residual oxide fraction.

The Co K-edge EXAFS and FT of $La_{10}Si_5CoO_{26.5}$ after reaction with NH_3 at 1000 °C (Fig. 13(b)) is different to that of $La_{9.67}Si_5CoO_{26}$ after reaction with NH_3 at 1000 °C (Fig. 13(a)) and cobalt metal (Fig. 13(d)), with the presence of a marked shoulder on the first peak in the FT. Using the hcp cobalt parameters, an initial fit confirmed the presence of cobalt metal, but with coordination numbers reduced to 50% of those in the bulk. When a Co–O interaction was included, this refined to a distance of 1.93(2) Å with an occupation number of 2, thus indicating the presence of a substantial quantity of oxide still present after heating to 800 °C. This is confirmed in the Co K-edge XANES spectrum of this sample (Fig. 9(d)), which has more features in common with the lower temperature sample (Fig. 7(c)) than does $La_{9.67}Si_5CoO_{26}$ after reaction with NH_3 at 1000 °C. The Debye–Waller factors are similar to those obtained from the spectra of $La_{9.67}Si_5CoO_{26}$ after reaction with NH_3 at 1000 °C indicating the same extent of amorphous character in both. This shell, together with the four cobalt shells, is included in Table 6 and Fig. 13(b)).

The Co K-edge EXAFS and FT of $La_{10}Ge_5CoO_{26.5}$ after reaction with NH_3 at 800 °C (Fig. 13(c)) is even more different when compared to the two silicate samples as there is very little evidence for the presence of the more distant Co…Co hcp shells. When the data were modelled using the same approach with a constant ratio of cobalt coordination numbers, a value of 44% was obtained. However, it is clear from the Debye–Waller factors in Table 6 and the data in Fig. 13(c) that the more distant shells are effectively no longer present. This behaviour is characteristic of the presence of very small particles, and based on our previous work may indicate particle sizes of 1–2 nm [33]. In addition to the small particle size, the inclusion of a Co–O shell was just about statistically significant, and this was included in the final fit with an occupation number of 1.4 and Co–O distance of 1.92(2) Å, which is the same as that observed for the 600 °C reduction sample.

Therefore, for all three of the samples there is evidence that the original apatites have undergone partial decomposition with the loss of cobalt metal. In the case of the silicates this results in relatively large amorphous particles, but for the germanate sample, the formation of small cobalt nanoparticles (1–2 nm) is indicated, as a result of the lower temperature at which the Co metal precipitates out from the lattice.

3.7. *Thermogravimetric analysis of ammoniated $La_{9.67}Si_5CoO_{26}$, $La_{10}M_5CoO_{26.5}$ (M=Si, Ge)*

Thermogravimetric analysis in O_2 was performed to determine the extent of nitrogen incorporation into the materials. Fig. 14 shows the TGA trace for $La_{9.67}Si_5CoO_{26}$, $La_{10}Si_5CoO_{26.5}$ and $La_{10}Ge_5CoO_{26.5}$ after reaction with ammonia at 800, 800 and 600 °C, respectively.

These data show a mass increase at ~300 and one at ~600 °C. Given the apparent reduction in cobalt oxidation state, shown by the XANES spectra, the former is tentatively attributed to reincorporation of O^{2-}, due to reoxidation of cobalt. The weight increase at ~600 °C is attributed to the substitution of two N^{3-} by three O^{2-} in line with previous studies of apatite systems not containing transition metals [11]. The resulting chemical formulae, calculated from TGA, are shown in Table 7.

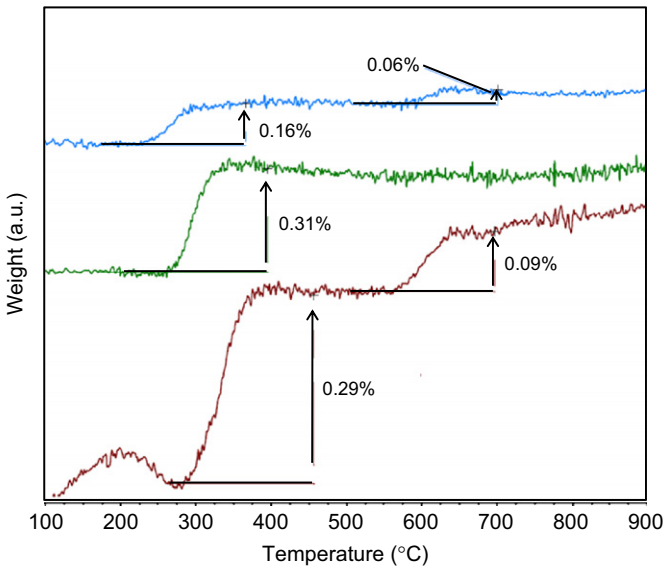

Fig. 14. TGA plots of $La_{9.67}Si_5CoO_{26}$ (green), $La_{10}Si_5CoO_{26.5}$ (brown) and $La_{10}Ge_5CoO_{26.5}$ (blue) after reaction with NH_3 at 800, 800 and 600 °C, respectively. (For interpretation of the references to color in this figure legend, the reader is referred to the web version of this article.)

The TGA trace of $La_{9.67}Si_5CoO_{26}$ shows no evidence of a weight increase at ~600 °C implying that there has been no N^{3-} incorporation upon ammonolysis. This may be related to the fact that this sample is normally oxygen stoichiometric, while the previous work on the $La_{8+x}Sr_{2-x}Si_6O_{26+x/2}$ systems suggested that the presence of oxygen excess was the driving force for the nitridation process. The weight increase at ~300 °C does, however, imply O^{2-} incorporation to reoxidise Co in the ammoniated sample. Assuming the 0.31% weight change is due to an anion deficiency, a stoichiometry of $La_{9.67}Si_5CoO_{25.62}$ is proposed for the ammoniated sample. It should also be noted that such a stoichiometry would imply a Co oxidation state of ~2.23+. This is consistent with the XANES data presented earlier, which showed a Co oxidation state close to 2+, but intermediate between 2+ and 3+.

Both the $La_{10}Si_5CoO_{26.5}$ and $La_{10}Ge_5CoO_{26.5}$ ammoniated samples show weight increase at approximately 300 and 600 °C. These increases are attributed to an O^{2-} deficiency in the ammoniated apatites and O^{2-}/N^{3-} substitution, respectively. A 0.09% mass increase in the TGA pattern of the ammoniated $La_{10}Si_5CoO_{26.5}$ sample suggests that, in the 375–550 °C range of the TGA, the stoichiometry of the sample is $La_{10}Si_5CoO_{26.23}N_{0.18}$. The 0.29% increase, associated with O^{2-} incorporation alone, implies a final stoichiometry of $La_{10}Si_5CoO_{25.87}N_{0.18}$ for the reaction of $La_{10}Si_5CoO_{26.5}$ with ammonia at 800 °C. The Co oxidation state of ~2.28+, this implies, is consistent with the XANES analysis. In addition, the oxidation states of ~2.23+ and ~2.28+, for ammoniated $La_{9.67}Si_5CoO_{26}$ and $La_{10}Si_5CoO_{26.5}$, respectively, support the similarity in edge position observed in the XANES.

Similarly, the mass increase of 0.06%, at 600 °C, and 0.16%, at 300 °C, for the $La_{10}Ge_5CoO_{26.5}$ ammoniated samples yields an intermediate (~375–550 °C) stoichiometry of $La_{10}Ge_5CoO_{26.30}N_{0.13}$ and a final formula of $La_{10}Ge_5CoO_{26.08}N_{0.13}$. This formula implies an oxidation state of ~2.55+. This is supported by XANES analysis and is consistent with the difference in edge position seen between the isostructural $La_{10}Si_5CoO_{26.5}$ and $La_{10}Ge_5CoO_{26.5}$ upon reaction with ammonia at 800 and 600 °C, respectively.

The Co substituted apatites, therefore, show far less N^{3-} uptake upon ammonolysis than the unsubstituted samples,

Table 7
Compositions for $La_{9.67}Si_5CoO_{26}$, $La_{10}M_5CoO_{26.5}$ (M=Si, Ge) samples after heating in NH_3.

Reaction conditions	Weight increase (%)	Chemical formula (~375–550 °C)[a]	Weight increase (%)	Chemical formula (after ammonolysis)
$La_{9.67}Si_5CoO_{26}+NH_3$ 800 °C	–	–	0.31	$La_{9.67}Si_5CoO_{25.62}$
$La_{10}Si_5CoO_{26.5}+NH_3$ 800 °C	0.09	$La_{10}Si_5CoO_{26.22(4)}N_{0.19(3)}$	0.29	$La_{10}Si_5CoO_{25.84(1)}N_{0.19(3)}$
$La_{10}Ge_5CoO_{26.5}+NH_3$ 600 °C	0.06	$La_{10}Ge_5CoO_{26.32(4)}N_{0.12(3)}$	0.16	$La_{10}Ge_5CoO_{26.10(2)}N_{0.12(3)}$

[a] Chemical formula proposed for the intermediate composition within the ~300–550 °C range of the TGA patterns.

instead favouring reduction of the cobalt metal through loss of O^{2-} anions. [10,11] The result of such low N^{3-} uptake is that overall anion content does not reach values significantly below 26 in the three samples, $La_{9.67}Si_5CoO_{25.62}$, $La_{10}Si_5CoO_{25.87}N_{0.18}$ and $La_{10}Ge_5CoO_{26.08}N_{0.13}$.

4. Conclusions

In this and previous studies it has been shown that all apatites, $La_{9.33}Si_6O_{26}$, $La_{8+x}Sr_{2-x}M_6O_{26+x/2}$ (M=Si, Ge; $0 \le x \le 2$), $La_{9.67}Si_5CoO_{26}$ and $La_{10}M_5CoO_{26.5}$ (M=Si, Ge), undergo reaction at the high temperatures with ammonia. For samples not containing transition metals, the key process is O/N exchange, while for the Co-doped samples, partial reduction of Co appears to be the dominant process. The extend of O/N exchange is linked to the presence of hyperstoichiometric oxygen in the starting apatite oxide and it was therefore more pronounced in $La_{8+x}Sr_{2-x}M_6O_{26+x/2}$ and $La_{10}M_5CoO_{26.5}$. In all cases, the Si-based apatites are shown to be more structurally stable than corresponding germanates after reactions at higher temperatures in ammonia.

As noted previously, the removal of interstitial oxide ions is likely to be detrimental to performance. Indications, therefore are that use of apatite electrolytes with ammonia as a fuel be limited to lower temperatures (<500 °C), at which nitrogen uptake is negligible, to prevent adverse effects of fuel on the performance. Furthermore, the partial substitution of the group 14 element by a transition metal seems to discourage O^{2-}/N^{3-} substitution in favour of the competing process, i.e. the reduction of the metal.

These studies highlight the importance of further studies on the influence of ammonia on SOFC electrolytes for use with ammonia fuel cells.

Acknowledgments

A. Orera and P.R. Slater would like to thank EPSRC for funding (Grant EP/F015178/1). The Netzsch thermal analyser used in this research was obtained through the Science City Advanced Materials project: Creating and Characterising Next generation Advanced Materials project, with support from Advantage West Midlands (AWM) and part funded by the European Regional Development Fund (ERDF). D.A. Headspith and M.G. Francesconi would like to thank the Leverhulme Trust for funding (Grant F/00 181/L). STFC are thanked for access to the Synchrotron Radiation Source at Daresbury Laboratory, and for the contribution that the SRS staff made to this work. NAY would like to thank Prof. S. Woodward (University of Nottingham) for providing the standard Co3,5-^{t}Bu-Cysalen[((R,R)-(-)-N,N'-bis(3,5-Di-t-butylsalicylidene)-1,2-cyclohexanediamino)cobalt(II)].

References

[1] A. Orera, P.R. Slater, Chem. Mater. 22 (2010) 675.
[2] N. Maffei, L. Pelletier, J.P. Charland, A. McFarlan, J. Power Sources 140 (2005) 264.
[3] A. McFarlan, L. Pelletier, N. Maffei, J. Electrochem. Soc. 151 (2004) A930.
[4] J. Staniforth, R.M. Ormerod, Green Chem. 5 (2003) 606.
[5] G. Meng, G. Ma, Q. Ma, R. Peng, X. Lui, Solid State Ionics 178 (2007) 697.
[6] R. Marchand, Y. Laurent, J. Guyader, P. L'Haridon, P. Verdier, J. Eur. Ceram. Soc. 8 (1991) 197.
[7] S.J. Clarke, K.A. Hardstone, C.W. Michie, M.J. Rosseinsky, Chem. Mater. 14 (2002) 2664.
[8] M. Ni, M.K.H. Leung, D.Y.C. Leung, Int. J. Energy Res. 33 (2009) 943.
[9] A. Belen-Jorge, J. Fraxedas, A. Cantarero, A.J. Williams, J. Rogers, J.P. Attfield, A. Fuertes, Chem. Mater. 20 (2008) 1682.
[10] E. Kendrick, D. Headspith, A. Orera, D.C. Apperley, R.I. Smith, M.G. Francesconi, P.R. Slater, J. Mater. Chem. 19 (2009) 749.
[11] A. Orera, D. Headspith, D.C. Apperley, M.G. Francesconi, P.R. Slater, J. Solid State Chem. 182 (2009) 3294.
[12] S. Nakayama, H. Aono, Y. Sadaoka, Chem. Lett. (1995) 431.
[13] S. Nakayama, M. Sakamoto, M. Higuchi, K. Kodaira, J. Mater. Sci. Lett. 19 (2000) 91.
[14] J.E.H. Sansom, D. Richings, P.R. Slater, Solid State Ionics 139 (2001) 205.
[15] L. Leon-Reina, E.R. Losilla, M. Martinez-Lara, S. Bruque, M.A.G. Aranda, J. Mater. Chem. 14 (2004) 1142.
[16] E. Kendrick, M.S. Islam, P.R. Slater, J. Mater. Chem. 17 (2007) 3104.
[17] B. Rhodes, S. Rowling, P. Tidswell, S. Woodward, S.M. Brown, J. Mol. Catal. A: Chem 116 (1997) 375.
[18] N. Binsted, in: PAXAS: Program for the Analysis of X-ray Absorption Spectra, The University of Southampton, 1988.
[19] A. Tenderholt, B. Hedman, K.O. Hodgson, PySpline: a modern, cross-platform program for the processing of raw averaged XAS edge data: X-ray absorption fine structure—XAFS 13, eds. B. Hedman and P. Paianetta, AIP Conference Proceedings 2007.
[20] EXCURV98, CCLRC Daresbury Laboratory Computer Program, CCLRC, Daresbury Laboratory, UK, 1998.
[21] T. Iwata, K. Fukuda, E. Bechade, O. Masson, I. Julien, E. Champion, P. Thomas, Solid State Ionics 178 (2007) 1523.
[22] S.S. Pramana, W.T. Klooster, T.J. White, Acta Cryst. B 63 (2007) 597.
[23] S.S. Pramana, W.T. Klooster, T.J. White, J. Solid State Chem. 181 (2008) 1717.
[24] J.R. Tolchard, J.E.H. Sansom, M. Saiful Islam, P.R. Slater, Dalton Trans. (2005) 1273.
[25] O. Haas, R.P.W.J. Struis, J.M. McBreen, J. Solid State Chem. 177 (2004) 1000.
[26] A.D.J. Barnes, T. Baikie, V. Hardy, M.B. Lepetit, A. Maignan, N.A. Young, M.G. Francesconi, J. Mater. Chem. 16 (2006) 3489.
[27] H.S.C. O'Neill, Mineral. Mag. 67 (2003) 547.
[28] V.P.S. Awana, S.K. Malik, W.B. Yelon, M. Karppinen, H. Yamauchi, Physica C 378–382 (2002) 155.
[29] G.J. Colpas, M.J. Maroney, C. Bagyinka, M. Kumar, W.S. Willis, S.L. Suib, N. Baidya, P.K. Mascharak, Inorg. Chem. 30 (1991) 920.
[30] J.R. Tolchard, M.S. Islam, P.R. Slater, J. Mater. Chem. 13 (2003) 1956.
[31] T.A. Smith, J.E. Penner-Hahn, M.A. Berding, S. Doniach, K.O. Hodgson, J. Am. Chem. Soc. 107 (1985) 5945.
[32] S.H. Baker, M. Roy, S. Louch, C. Binns, J. Phys.: Condens. Matter 18 (2006) 2385.
[33] F. Cheng, S.M. Kelly, N.A. Young, C.N. Hope, K. Beverley, M.G. Francesconi, S. Clark, J.S. Bradley, F. Lefebvre, Chem. Mater. 18 (2006) 5996.